Optical model for use in oceanic ecosystem models

Cheng-Chien Liu, John D. Woods, and Curtis D. Mobley

Modeling the plankton ecosystem requires a code for simulating the profile of irradiance from the chlorophyll profile at each time step of the integration. We have compared two existing codes with data from the Biogeochemical Ocean Flux Study: the Hydrolight radiative transfer model is accurate but too slow to use interactively in ecological models; Morel's [J. Geophys. Res. **93,** 10,749 (1988)] empirical model is much faster but produces substantial error. We have developed a streamlined version of the Hydrolight radiative transfer model that is 20 times faster than the full Hydrolight code, while limiting errors to less than 12% within the euphotic zone. This new code is both fast and accurate and is, therefore, suitable for use interactively in oceanic ecosystem models. © 1999 Optical Society of America

OCIS codes: 010.0010, 010.4450.

1. Introduction

Realistic simulation of the marine plankton ecosystem is a prerequisite for assessing the impact of biology on a wide variety of important phenomena, including climate, water quality, and fisheries. Realism depends on accurately simulating the demographic histories of each plankton population. We computed these time series (for number/m^3, birth rate, death rate classified by cause of death, and life expectancy) by integrating a model comprising equations for the major processes. Five of the most important processes (heating, mixing, photosynthesis, diel migration, and visual predation) depend on the vertical profile of scalar irradiance $E_o(z)$, which itself changes with the plankton demography. Accurate calculation of $E_o(z)$ is essential if the simulated ecosystem is to describe the plankton demography realistically. In practice a high computational cost is incurred in achieving sufficient accuracy in $E_o(z)$ for even modest demographic goals (e.g. timing of the spring bloom to plus or minus one day). We shall see later that adding realistic optical modeling to ecological simulation can increase integration time by a factor of many thousands. This is normally unacceptable, so current practice for computing $E_o(z)$ within plankton ecology models falls far short of such goals because of the limited computer power available. In practice, plankton ecologists make do with computationally cheap but error-prone codes for determining $E_o(z)$ as a dynamic variable within their ecological models.

The optical model generally used in various physical–biological models was developed by Morel.[1] This model allows for the propagation of visible radiant energy within the ocean to be rapidly predicted as a function of the local phytoplanktonic content. Therefore, it is suited for the repeated irradiance computation when simulating the physical–biological interaction of the plankton ecosystem in the long term. Various numerical optical models were also developed for computing light distributions both above and below the ocean surface by solving the radiative transfer equation (RTE). Mobley *et al.*[2] made a comprehensive comparison of these models and concluded that these models provide accurate numerical solutions for most of the needs of optical oceanography and limnology. However, the computation time required for these numerical optical models is long. There is no research that compares the accuracy of the empirical optical model with the numerical optical models, nor on the feasibility of embedding the numerical optical models into physical–biological plankton models.

Here we aim to assess both the Morel empirical and the Hydrolight[3–6] numerical optical models using the Biogeochemical Ocean Flux Study (BOFS) data collected in 1990. The measured chlorophyll profiles, together with the meteorological conditions, are used as input to these two optical models to calculate the

C.-C. Liu and J. D. Woods are with the T. H. Huxley School of Environment, Earth Science and Engineering, Imperial College, London SW7 2AZ, UK. The e-mail address for J. D. Woods is j.woods@ic.ac.uk. C. D. Mobley is with Sequoia Scientific, Incorporated, 9725 S.E. 36th Street, Suite 308, Mercer Island, Washington 98040.

underwater irradiance distribution. These results are then compared to the measured irradiance profiles collected at the same time (on the CTD casts). They show that the Morel method leads to substantial error, whereas the error in using Hydrolight is much less. Nevertheless, it is common practice in ecological modeling to use the former because it is much faster. Our aim is to find a way to accelerate Hydrolight without significant loss of accuracy. The feasibility of embedding the numerical optical model into a physical–biological plankton model is also investigated. The computation time of the numerical optical model can be reduced dramatically by applying the numerical computation conditions determined by the same *in situ* measurement.

2. Biogeochemical Ocean Flux Study Data

The *in situ* data were collected during the Charles Darwin 46 cruise mounted by the BOFS project at the Lagrangian station at approximately 50°N 20°W from April to May in 1990. These process cruises continuously sampled the water column almost daily. In addition, the underway data, including navigation, surface water information, meteorological conditions, and water depth, were monitored and logged every 30 s during each cruise. All the BOFS data were managed and archived as the BOFS North Atlantic data set[7] by the British Oceanographic Data Centre.

The CTD profiles including chlorophyll and downwelling and upwelling scalar irradiance were taken with a Research Vessel Services Neil Brown Systems Mk3B CTD, which was mounted vertically in the center of a protective cage approximately 1.5 m square and lowered at between 0.5 and 1.0 m/s. The chlorophyll concentration was measured by a Chelsea Instrument Aquatracke fluorometer, which was calibrated in terms of chlorophyll with a multiple regression technique against extracted chlorophyll and downwelling scalar irradiance. Because the ship was a holding station on a drifting buoy, the chlorophyll data from the entire cruise were treated as a single population. Two Polymouth Marine Laboratory 2-pi photosynthetically available radiation (PAR) sensors were separated vertically by 2 m to measure the downwelling and upwelling wavelength-integrated scalar irradiance (PAR), respectively. It should be noted that these hemispherical domed sensors measured the scalar irradiance rather than the planar irradiance.

The Charles Darwin 46 cruise yielded 27 profiles with the data needed for this study. We selected six of these to cover the full range of cloudiness and zenith angles. All the underway data including time, location, surface wind speed, chlorophyll concentration, and solar radiation were averaged within each CTD downcast event. Additional information, such as the depth of the mixing layer and the euphotic zone were also recorded. The solar zenith angle was calculated according to the given date, time, latitude, and longitude. The cloudiness was estimated from the difference between the theoretical clear-sky and the observed above-surface down-welling irradiances $E_d(0^+)$. The theoretical values were estimated by multiplying the solar constant by the cosine of the solar zenith angle and then by removing a proportion to account for transmission loss through the atmosphere[8] (14% for an overhead Sun, proportionately more for longer path lengths when the Sun is lower in the sky). It should be noted that these theoretical values are summed over all wavelengths, not just those of the PAR. The observed data that covered the entire spectrum were collected by the Kipp and Zonen type CM5/6 solarimeters.

The derived cloudiness and the above-surface irradiance $E_d(0^+)$, together with all the averaged underway data for each CTD downcast event, are listed in Table 1. Six sets of CTD profiles including chlorophyll concentration and upwelling and downwelling irradiance are plotted in Fig. 1. These profiles were selected to include both large and small Sun zenith angles under overcast or clear-sky conditions.

3. Optical Models

As mentioned above, the optical model generally used in various physical–biological models[9–11] was developed by Morel.[1] By analyzing the optical and related biological data acquired during several cruises in oceans in different parts of the world, Morel derived a spectral optical model that comprised the statistical relationships between the chlorophyll-like pigment concentration C and the downwelling irradiance

$$E_d(z; \lambda) = E_d(0^+; \lambda)\exp\left\{-\int[k_w(\lambda) + \chi_c(\lambda)C(z)^{e(\lambda)}]\mathrm{d}z\right\}.$$

(1)

The spectral values of the coefficients $\chi_c(\lambda)$, $e(\lambda)$, and the water attenuation coefficient $k_w(\lambda)$ are given in Table 2 of Morel's paper.[1] This spectral model is more accurate than the nonspectral models of light attenuation and photosynthesis, which can overestimate daily primary production in the water column by as much as 50% or more.[12] However, there is no parameter that describes the sky radiance distribution and takes into consideration the underwater scattering effect explicitly. Further investigation is needed to apply this model to various incident solar conditions such as a large Sun zenith angle or a heavily overcast day, and to the depth where the scattering effect dominates, compared with the absorption effect. In addition, the upwelling irradiance cannot be obtained from this model.

Various numerical optical models were developed for computing radiance $L(\hat{\xi}; \lambda)$ in the ocean by solving the RTE[13]:

$$\frac{\mathrm{d}L(\hat{\xi}; \lambda)}{\mathrm{d}r} = -c(\hat{\xi}; \lambda)L(\hat{\xi}; \lambda) + \int_{\Xi} L(\hat{\xi}'; \lambda)\beta(\hat{\xi}' \rightarrow \hat{\xi})\mathrm{d}\Omega(\hat{\xi}'),$$

(2)

where $c(\hat{\xi}; \lambda)$ is the attenuation coefficient, Ξ represents all directions $\hat{\xi}'$ in a unit sphere, and $\mathrm{d}\Omega(\hat{\xi}')$ is a

Table 1. BOFS CD46 Data Descriptions[a]

OID	0305C#4	0405C#8	0605C#6	1105C#6	1305C#3	1905C#2
BEN	7036	7329	7886	9177	9640	11131
DCSTART	1990/3/5	1990/4/5	1990/6/5	1990/11/5	1990/13/5	1990/19/5
	17:10	15:56	17:16	16:14	11:51	12:56
DCEND	1990/3/5	1990/4/5	1990/6/5	1990/11/5	1990/13/5	1990/19/5
	17:16	16:05	17:26	16:19	11:59	13:08
Time	17.22	16.01	17.34	16.28	11.92	12.98
Latitude	49.93	49.85	49.61	49.31	49.13	48.52
Longitude	-18.45	-18.52	-18.47	-18.23	-17.77	-17.38
V_{wind}	7.72	18.67	12.21	17.34	15.63	10.51
Chl(0)	1.07	1.20	1.34	1.43	1.15	1.32
$E_{od}(0^{+})$(PAR)	87.49	197.82	82.54	168.03	477.45	538.56
$E_{d}(0^{+})$(total)	135.22	325.62	127.46	257.92	875.89	896.3
MLD	-1	-1	22.8	12.9	22.8	5
EZD	28.2	26.5	23.8	22.6	23.8	22.6
θ_{Sun}	59.49	48.31	59.94	49.04	34.19	28.96
Cloud	73.22	54.83	74.28	63.56	7.17	11.18
$E_{d}(0^{+})$(PAR)	40.67	111.38	38.48	93.87	477.45	378.08

[a]OID, originator identifier; BEN, BODC event number; DCSTART, downcast start time (Greenwich Mean Time); DCEND, downcast end time (Greenwich Mean Time); V_{wind}, surface wind speed (knots); chl(0), surface chlorophyll concentration (mg m^{-3}); $E_{od}(0^{+})$(PAR), above-surface downwelling scalar irradiance in the PAR range, measured by the Polymouth Marine Laboratory 2-pi PAR sensors (W m^{-2}); $E_{d}(0^{+})$(total), above-surface downwelling scalar irradiance summed over the whole spectrum, measured by the Kipp and Zonen type CM5/6 solarimeters (W m^{-2}); MLD, mixing layer depth (m); EZD, euphotic zone depth (m); θ_{Sun}, Sun zenith angle (deg); cloud, cloudiness (%); $E_{d}(0^{+})$(PAR), above-surface downwelling planar irradiance in the PAR range (W m^{-2}).

differential element of solid angle centered on $\hat{\xi}'$. The volume scattering phase function $\beta(\hat{\xi}' \to \hat{\xi})$ defines the contribution of the radiances scattered from all directions $\hat{\xi}'$ toward the direction $\hat{\xi}$. The RTE describes that the rate of change of radiance L in the direction $\hat{\xi}$ through a distance r is the combination of loss that is due to attenuation and gain that is due to scattering. The water body discussed in hydrologic optics is infinite in horizontal extent and there are no horizontal variations of inherent optical properties (IOP's) or of boundary conditions. However, the IOP's can vary arbitrarily with depth, therefore the spatial variables of the IOP's can be reduced to one, that is depth z. The RTE can be written as

$$\mu \frac{dL(z; \hat{\xi}; \lambda)}{dz} = -c(z; \lambda) L(z; \hat{\xi}; \lambda)$$
$$+ \int_{\Xi} L(z; \hat{\xi}'; \lambda)\beta(z; \hat{\xi}' \to \hat{\xi}; \lambda)d\Omega(\hat{\xi}').$$
(3)

Note that the increment of path length is expressed as $dr = dz/\cos \theta = dz/\mu$, because $z = r \cos \theta$. By introducing the single-scattering albedo $\omega_0 = b/c$, the normalized volume-scattering function $\tilde{\beta} \equiv \beta/b$, and the optical depth $\varsigma = \int_0^z c(z')dz'$, the dimensionless form of RTE can be expressed as

$$\mu \frac{dL(\varsigma; \hat{\xi}; \lambda)}{d\varsigma} = -L(\varsigma; \hat{\xi}; \lambda) + \omega_0(\varsigma; \lambda)$$
$$\times \int_{\Xi} L(\varsigma; \hat{\xi}'; \lambda)\tilde{\beta}(\varsigma; \hat{\xi}' \to \hat{\xi}; \lambda)d\Omega(\hat{\xi}'). \quad (4)$$

Among the various numerical optical models, Hydrolight[4–6] is preferred because it is computationally extremely fast compared with other solution methods. Furthermore, unlike the Monte Carlo method, which suffers from statistical noise, the invariant embedding technique used in Hydrolight computes all results with equal accuracy. The radiance $L(\varsigma; \hat{\xi}; \lambda)$ is a directional quantity, whereas the normalized volume-scattering function $\tilde{\beta}(\varsigma; \hat{\xi}' \to \hat{\xi}; \lambda)$ is a bidirectional quantity: convert one radiance into another radiance. Before applying the numerical invariant embedding technique, the infinite number of directions has to be reduced to a finite number by introducing a directional discretization, quad partition. Figure 2 illustrates an equal-angle partition of Ξ. All directional and bidirectional quantities can be quad averaged. In a manner of speaking, the quad-averaging process replaces the clear unit sphere by a polyhedron of frosted glass windows; each window makes the radiance distribution uniform within that window.[6] The integrodifferential equation (4) can be discretized by averaging over direction and wavelength as (Ref. 4, Sections 8.2 and 11.8)

$$\mu_u \frac{dL(\varsigma; u, v; l)}{d\varsigma} = -L(\varsigma; u, v; l) + \omega_0(\varsigma; l)$$
$$\times \sum_r \sum_s L(\varsigma; r, s; l)\tilde{\beta}(\varsigma; r, s \to u, v; l),$$
(5)

where $Q_{uv}, Q_{rs} \in \Xi$. This quad- and band-averaged RTE along with its boundary conditions are a set (typically hundreds) of ordinary differential equations, that can be solved by a high-order Runge–Kutta algorithm.

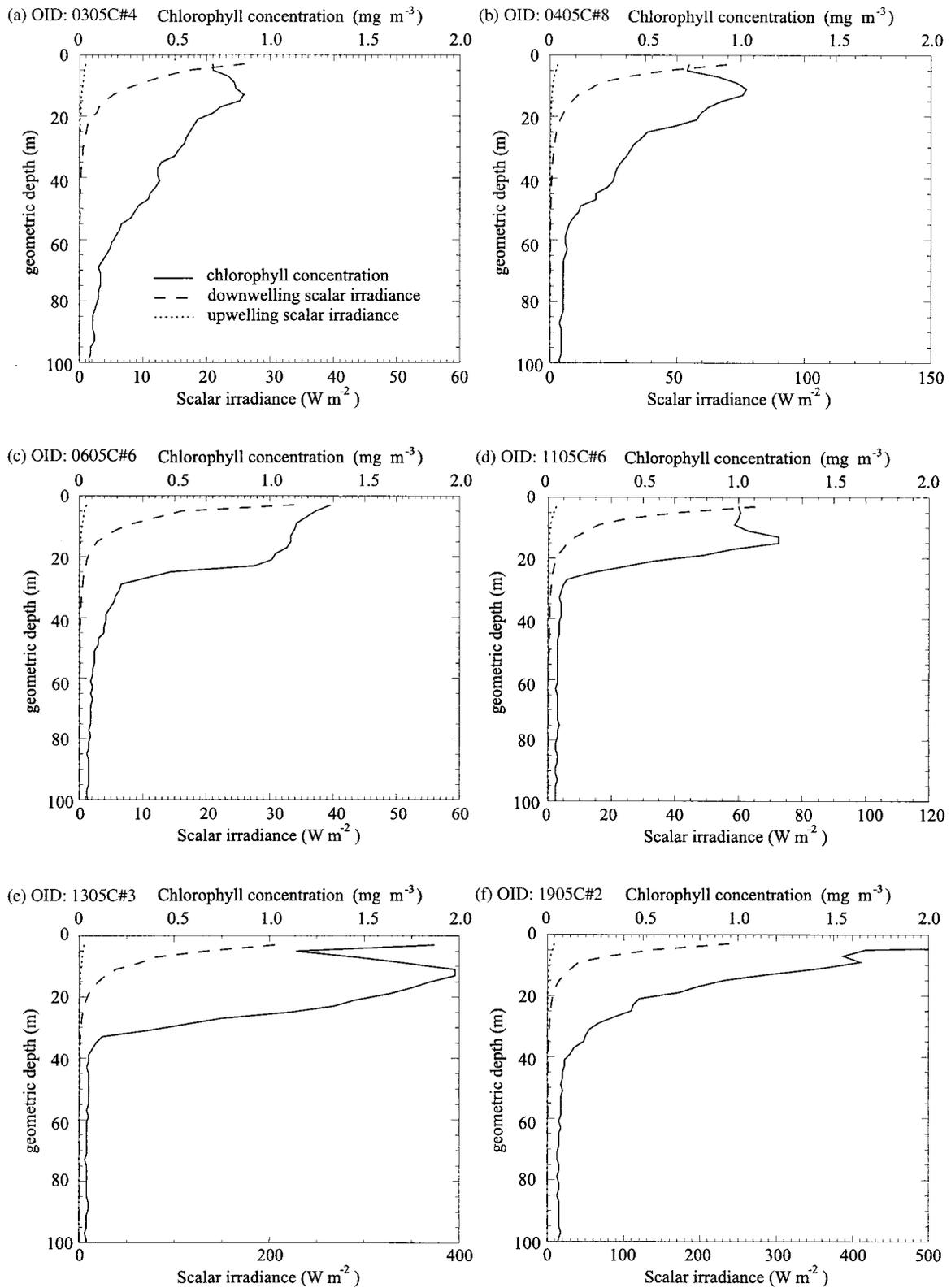The calculation procedures of Hydrolight can be

Fig. 1.   Chlorophyll and irradiance profiles collected on the CTD casts by the BOFS project in 1990.

grouped into three parts. First, the quad partition has to be selected. A Monte Carlo ray tracing method is then used to estimate four surface reflectance and transmittance functions that are needed to specify the air–water boundary conditions. This

time-consuming method is unavoidable because it is the only mathematically tractable way to simulate the radiative properties of random sea surfaces. Furthermore, this procedure has to be repeated for different surface wind speeds. Second, the scatter-

Table 2. Comparisons of the Computer Time Consumption and Deviations by Use of a Standard Numerical Condition and Various Relaxed Numerical Conditions to Simulate the Underwater Downwelling Planar Irradiance E_d

	———	----------	··············	—·—·—	—··—··
Quad partition	20×24	20×24	12×12	20×24	20×24	12×12
Wavebands in the PAR range	36	36	36	18	36	18
Maximum geometric depth Z_{max}	60	60	60	60	35	35
Quick reference database of the air–water boundary conditions and the scattering phase function	No	Yes	Yes	Yes	Yes	Yes
Computer time consumption (SGI challenge) (second)	7237	5515	582	2346	3238	172
Deviation (max value within euphotic zone) (%)			12.41	0.71	0.01	11.84
Deviation (max value within 60 m) (%)			17.12	0.71	1.27	17.90

ing phase functions for different constituents of sea-water are discretized according to the selected quad partition. The main constituent is chlorophyll because the site we focused on is categorized as case I water. All the IOP's can be obtained from analytical models[14,15] by taking constituents of seawater into consideration. The discretization calculations need to be performed only once for a selected quad partition. Finally, the air–water boundary conditions, the IOP's, and the input sky radiance determined by the above-surface irradiance $E_d(0^+)$ and cloudiness are used to solve the set of ordinary differential equations (5) for the quad- and band-averaged radiance. The other quantities, such as downwelling and up-welling planar irradiance or scalar irradiance, can be computed from the radiance.

A detailed description of equations and variables can be found in Ref. 4. Here we used Hydrolight Version 3.1 to compute the underwater irradiances. Our calculation focused on the open ocean, where the water can be reasonably regarded as infinitely deep. In addition, we ignored internal sources and inelastic scattering within the water body.
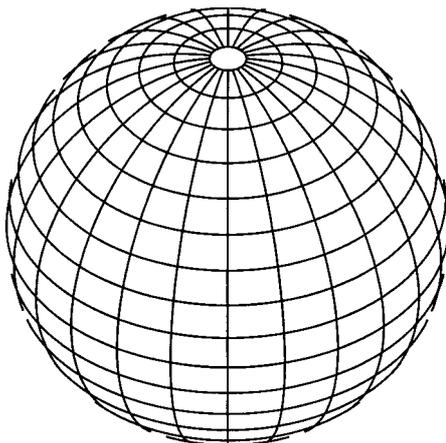

Fig. 2. Equal-angle partition of Ξ by means of circles of constant θ and by semicircles of constant ϕ. Based on Mobley, the number of quads in the θ direction is $M = 2m = 20$ and the number in the ϕ direction is $N = 2n = 24$. All nonpolar-cap quads have equal angular widths $\Delta\phi = 2\pi/N = \pi/n$, $\Delta\theta = \pi/M = \pi/2m$ and center at $\phi_v \equiv (v-1)\Delta\phi = (v-1)\pi/n$ for $v = 1, 2, \ldots, 2n$, and $\theta_u \equiv (u-1)\Delta\theta = (u-1)\pi/2m$ for $u = 1, 2, \ldots, 2m$.

4. Results

All the valid BOFS data listed in Table 1, together with the CTD chlorophyll profiles, are used in both Hydrolight and the Morel empirical model based on Eq. (1) to simulate underwater irradiance. These results are then compared with the upwelling and downwelling irradiance profiles collected *in situ*. The comprehensive comparisons show that the deviation between the Morel empirical model and the BOFS data is apparent at depths of 10 m and increases rapidly with depth, especially for a large Sun zenith angle or a heavily overcast day. In contrast, Hydrolight offers a simulation that corresponds more closely to the BOFS data throughout the entire euphotic zone, regardless of the incident sky radiance condition. The comparison results based on the six sets of CTD profiles (Fig. 1) are plotted in Fig. 3. Note that Hydrolight provides not only the scalar downwelling and upwelling irradiances E_{od} and E_{ou} but also the planar downwelling and upwelling irradiances E_d and E_u. Yet the BOFS data collected in 1990 measured only E_{od} and E_{ou} and the Morel empirical model can provide only E_d. To make a direct comparison between BOFS data and the results of optical models, the value of $E_{od}{}^*$ predicted by the Morel empirical model in Fig. 3 is converted from E_d according to

$$E_{od}{}^* = \frac{E_d}{\bar{\mu}_d},$$

where

$$\bar{\mu}_d = \cos\theta_w = \cos\left[\sin^{-1}\left(\frac{n_a}{n_w}\sin\theta_{Sun}\right)\right]. \qquad (6)$$

Equation (6) assumes that the average cosine of downwelling light $\bar{\mu}_d$ remains constant throughout the entire water column and is equal to the surface value calculated under the ideal incident condition, i.e., the collinear solar beam incident at θ_{Sun} without any background scattering. The nadir angle of the solar beam after it passes through the air–water surface θ_w is determined by Snell's law of refraction: $n_w \sin\theta_w = n_a \sin\theta_{Sun}$. This approach leads to overestimation of the values of $\bar{\mu}_d$ both at the surface and underwater, with the result that $E_{od}{}^*$ underesti-
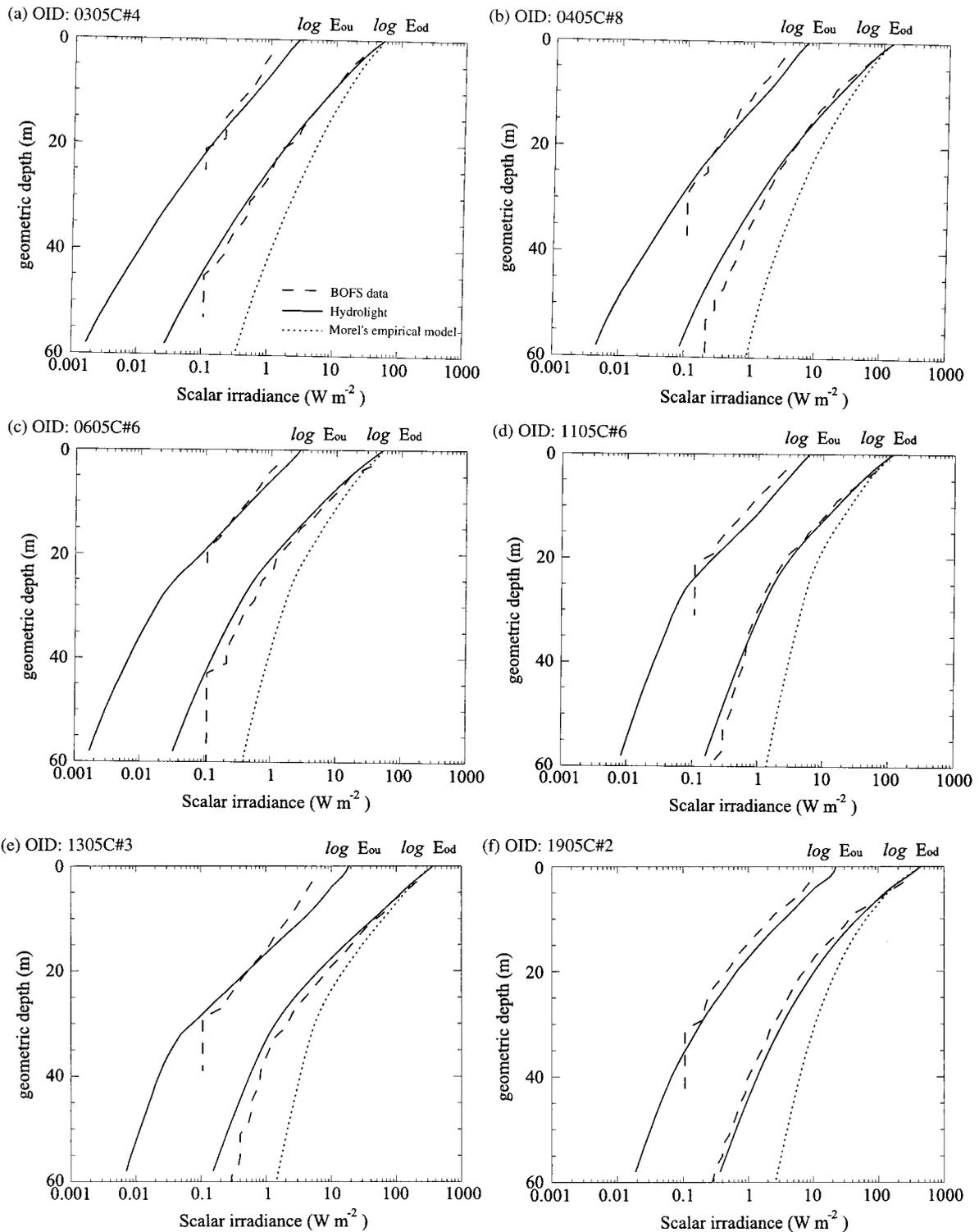
Fig. 3. Comparison of the wavelength-integrated underwater scalar irradiances between the BOFS measurements, Hydrolight, and the Morel empirical model. Note that the profile based on Morel's model uses E_{od}^* as a surrogate for E_{od}; see Eq. (6) and the accompanying discussion.

mates E_{od}. Inspection of Fig. 3 indicates that such underestimation also leads to underestimation of the difference between the irradiance profile derived for the BOFS measurements and Morel's method. Figure 4 gives a direct comparison of the values of E_d as

estimated by these two optical models. The accuracy of the empirical model is profoundly influenced by the scattering effect, especially under the large Sun zenith angle, of a heavily overcast day, and the deeper depth where the scattering effect dominates.

(a) OID: 0305C#4

(b) OID: 0405C#8

(c) OID: 0605C#6

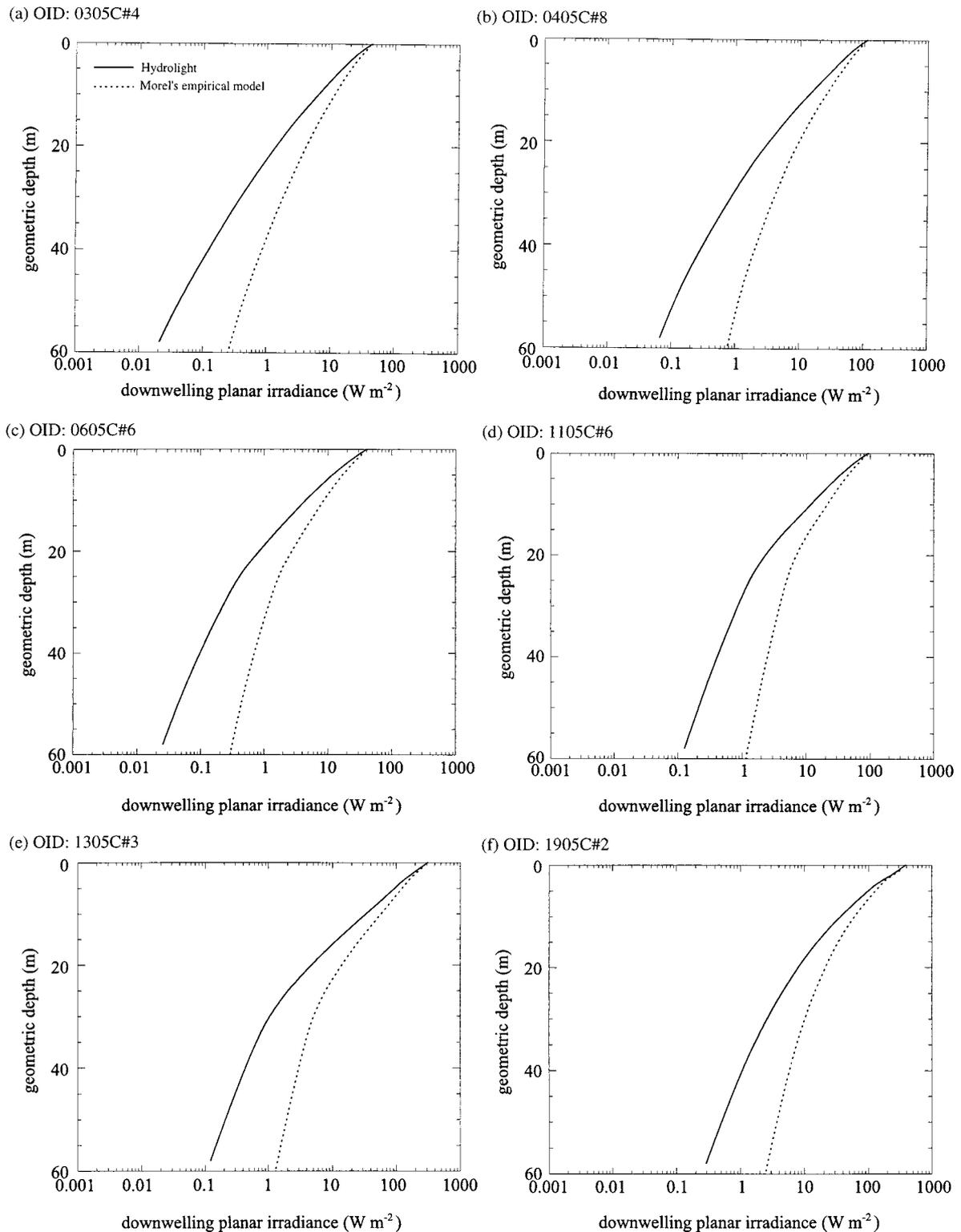**(d) OID: 1105C#6**

(e) OID: 1305C#3

(f) OID: 1905C#2

Fig. 4. Comparison of the wavelength-integrated underwater planar irradiances between Hydrolight and the Morel empirical model.

It should also be noted that, in relation to the absorption algorithm, only the chlorophyll concentration was measured in the BOFS project; there was no information about the concentrations of other components, such as gilvin (also known as yellow matter) or detritus. Therefore, one bio-optical absorption algorithm is used in the Hydrolight model to calculate the total absorption coefficient

$$a(z; \lambda) = [a_w(\lambda) + 0.06a_c{}^*(\lambda)C(z)^{0.65}]$$
$$\times \{1 + a_{\text{other}} \exp[-0.014(\lambda - 440)]\}. \quad (7)$$
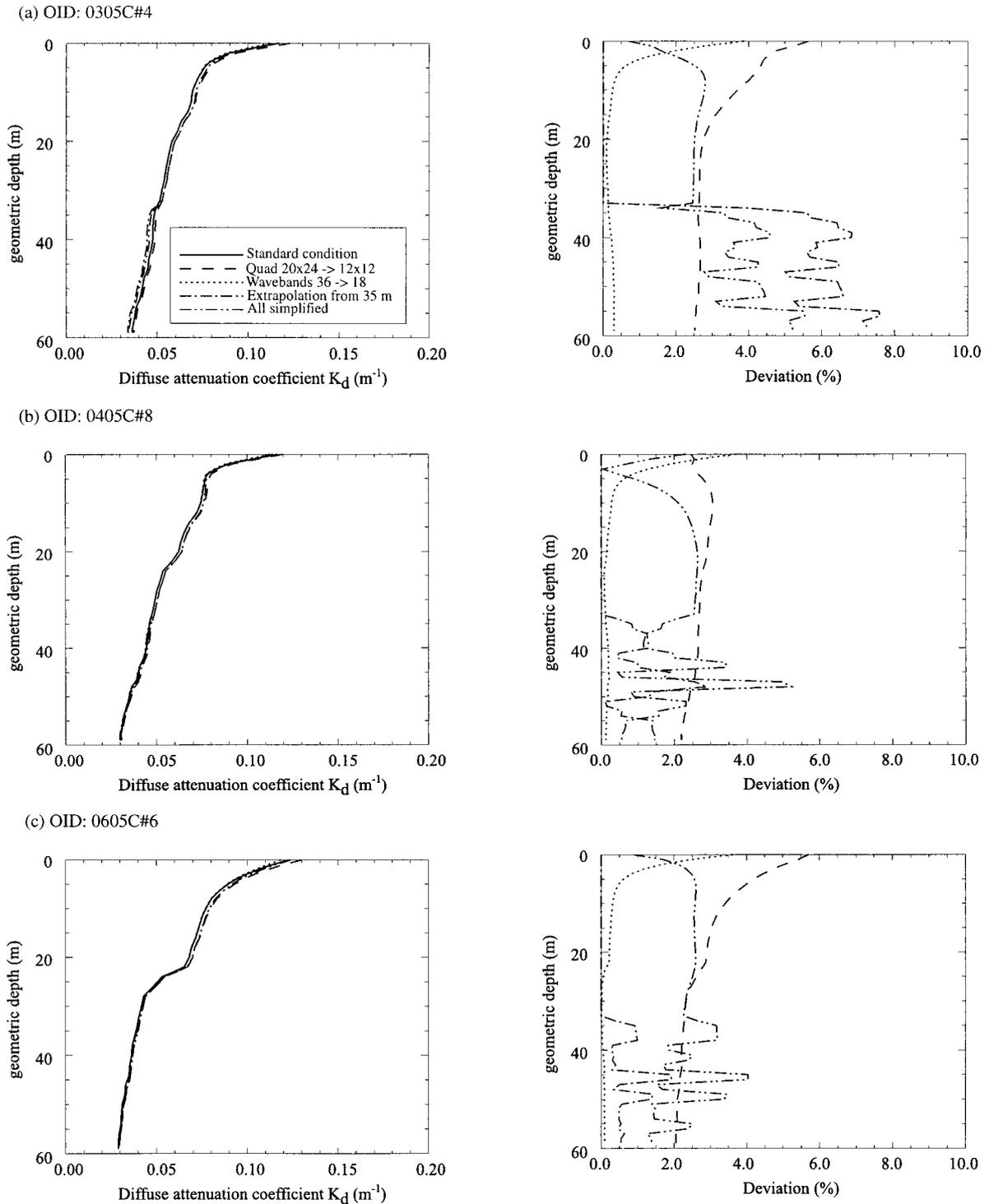
(a) OID: 0305C#4

(b) OID: 0405C#8

(c) OID: 0605C#6

Fig. 5. Sensitivity test of Hydrolight to various conditions. Simulations on the diffuse attenuation coefficient for the downwelling planar irradiance K_d obtained with the standard numerical condition and various relaxed numerical conditions for BOFS originator identifier (OID) data (a) 0305C#4, (b) 0405C#8, (c) 0605C#6.

This algorithm[15,16] assumes that a fixed percentage of the total absorption at a given wavelength always comes from yellow matter and $a_{other} \equiv a_g = 0.2$. In this study, the model-data fit is attempted to determine inversely the total contribution from other components. The best fits of model results and data were obtained with $a_{other} = 0.8$. Although the model was partially tuned to obtain the best model-data fit, the same value of a_{other} was applied to each CTD event. In other words, the ability of the Hydrolight model to give reasonable predictions simultaneously for each CTD event is due to correct representation of the underlying dynamics rather than to adjusting parameter values for each event. The same ap-
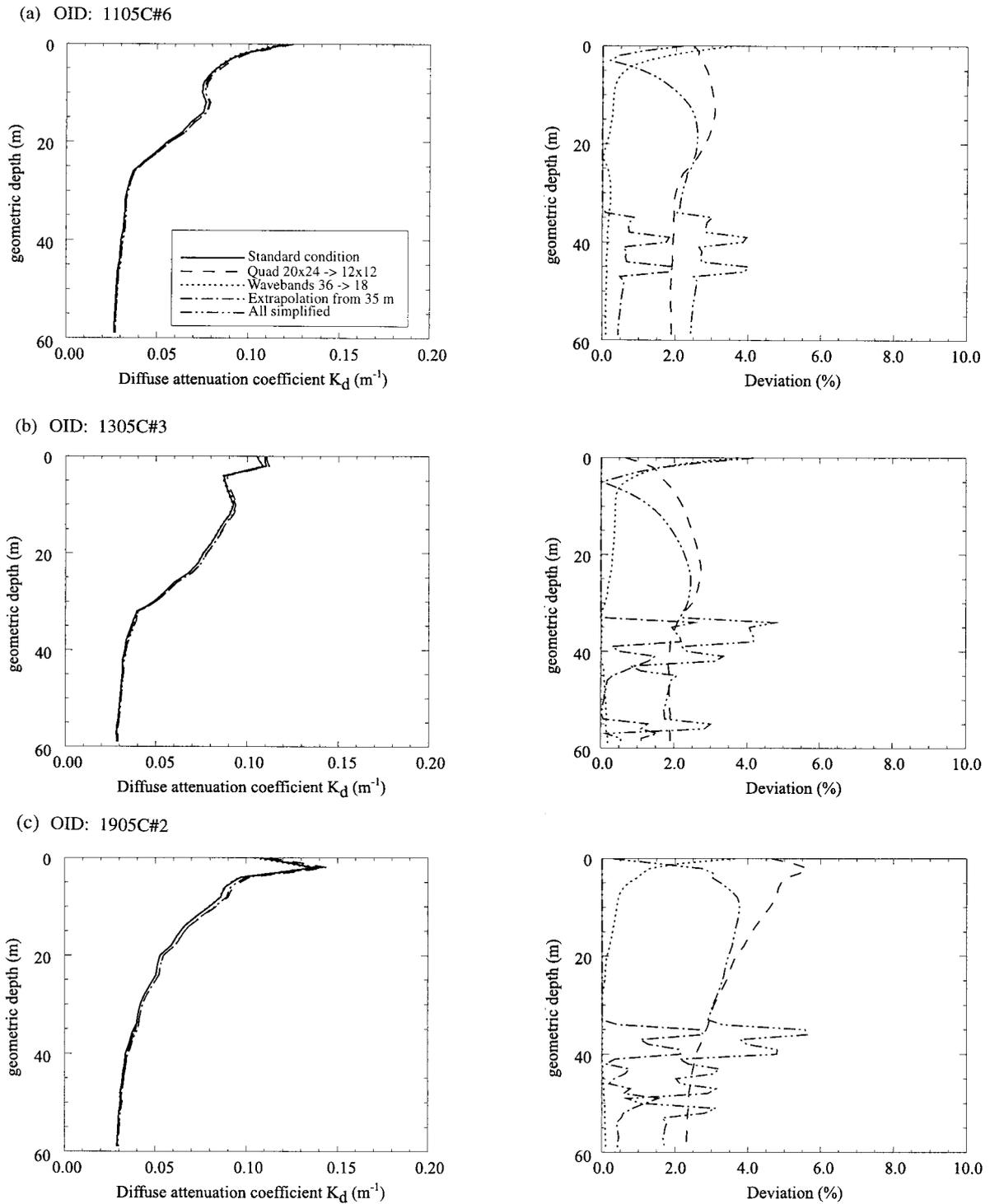
Fig. 6. Sensitivity test of Hydrolight to various conditions. Simulations on the diffuse attenuation coefficient for the downwelling planar irradiance K_d obtained with the standard numerical condition and various relaxed numerical conditions for BOFS originator identifier (OID) data (a) 1105C#6, (b) 1305C#3, (c) 1905C#2.

proach of parameterization has been used by Tyrrell et al.[17]

The simulation of the Hydrolight model was integrated on an SGI Challenge computer that has four 200-MHz processors. Each simulation was executed by one processor. Elapsed time for each run was recorded for comparison. The numerical conditions for each simulation were wavebands $n_{wave} = 36$ within the PAR range; equal-angle quad-partition $M \times N = 20 \times 24$ and the maximum geometric depth $z_{max} = 60$ m. It took approximately 15 min to calculate the air–water boundary conditions; 13 min to discretize the scattering phase function, and 92 min to compute the underwater light field. Hydrolight is much faster

than Monte Carlo models, which might need months of computer time to achieve the same accuracy to the same depth.[18] However, requiring 120 min of computer time for each simulation, it is still far beyond present computer technology to support repeated calculations required for the simulation of a plankton ecosystem in the long term. For example, it would take approximately two years of computer time to simulate the annual variation of a plankton ecosystem by use of a physical–biological plankton model with a 0.5-h time step.

To reduce the computation time without losing accuracy, three procedures were used to find the streamlined numerical conditions for simulating the underwater irradiance. First, the quad partition and wavebands were relaxed to $M \times N = 12 \times 12$ and $n_{\mathrm{wave}} = 18$ within the PAR range because the physical–biological plankton model is concerned only with the scalar downwelling and upwelling irradiances that are computed from integrals of the radiance over direction and over the PAR range. The Hydrolight model is not sensitive to the quad partition when it is used to calculate the underwater irradiance. Second, a quick reference database of the air–water boundary conditions and the scattering phase function can be established in advance and save at least one third of the computation time in a repeated long-term simulation, since they need to be computed only once for a selected quad partition and surface wind speed. Finally, because the plankton are abundant within z_m, by gradually decreasing to a depth of z_c and maintaining a small constant level below z_c, we were able to specify the maximum geometric depth z_{max} to a depth of z_c if the chlorophyll profile were already known, and we extrapolated all the irradiance below z_c with the results calculated at z_c. In other words, the maximum geometric depth z_{max} can be selected as a lower value during the spring bloom, when the plankton are abundant and little light can penetrate to greater depths. All the standard numerical conditions of the Hydrolight model used for the simulation in Fig. 3 are relaxed one by one. Sensitivity tests of Hydrolight to different conditions based on the set of six BOFS profiles (Fig. 1) are presented in Figs. 5 and 6. These figures show the simulations of the diffuse attenuation coefficient for the downwelling planar irradiance K_d that were obtained with the standard numerical condition and various relaxed numerical conditions. With this test we have demonstrated that the effectiveness of our streamlining of Hydrolight is equally valid over the wide range of ecological conditions encountered in the BOFS profiles (Fig. 1); the additional error arising from use of our simplification never exceeded 8% in this set of profiles. Figure 7 gives the downwelling planar irradiance E_d of BODC event 9177 (OID: 1105C#6) on 11 May 1990 obtained with various numerical conditions. The computer time consumption for each relaxation computation and the deviation from the standard calculation are listed in Table 2. This comparison indicates that the computation time, after applying all the relaxation conditions, can be reduced by at least 95% without introducing a deviation of greater than 12% within the euphotic zone.
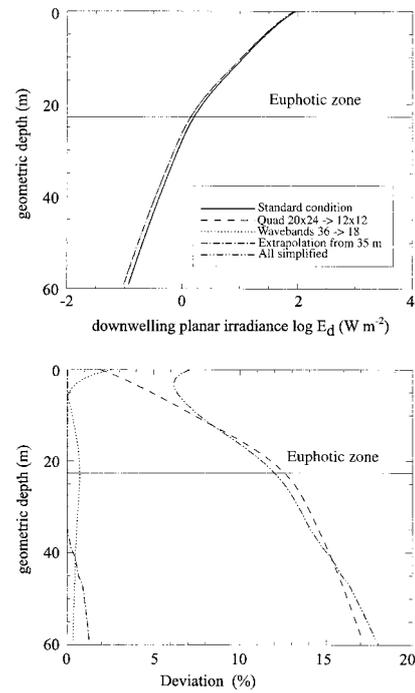

Fig. 7. Comparison of the underwater downwelling planar irradiance E_d made with the standard numerical condition and various relaxed numerical conditions.

5. Discussion

We assessed two optical models, the Morel empirical model and the Hydrolight numerical model, by using the BOFS data collected in the North Atlantic Ocean in 1990. The comparisons indicate that the empirical model is not valid for some incident light conditions, especially for a large Sun zenith angle, on a heavily overcast day, or at deeper depths where the scattering effect dominates. On the other hand, Hydrolight provides an accurate simulation throughout the euphotic zone, regardless of the incident sky radiance condition. This research suggests that the physical–biological plankton models, all of which use the empirical bio-optical model to calculate underwater irradiance, need to be reexamined.

The feasibility of embedding the Hydrolight optical model into a physical–biological plankton model is investigated. Several strategies such as quad-partition relaxation and extrapolation are used, together with the incorporation of a quick reference database, resulting in a 95% reduction of computation time without introducing a deviation of more than 12%. These results encourage the adoption of a streamlined version of the Hydrolight model for simulating the optical environment in physical–biological plankton models.

The irradiances in the BOFS data set, as in most of the other data sets, are not sufficient for the purpose of studying the detailed underwater radiance, checking closure relations, or testing the accuracy of radiative transfer predictive models. The ideal measurements should be of high accuracy and simultaneously cover the entire range of IOP's and external lighting and boundary conditions found in nature. Unfortunately, such compre-

hensive data sets do not exist to date.[4] Nevertheless, if we take into consideration all the available data collected by the BOFS cruises, this research successfully assesses the underwater irradiance predicted by the two optical models and corroborates that Hydrolight provides a rapid and accurate simulation for most of the needs of optical oceanography and limnology.

Another potential application of this research is in visual ecology. The light distribution in the water not only affects the physical properties such as heat or density, but also influences the biological properties such as photosynthesis or migration. In the same way that many land creatures hide from predators' attacks by means of camouflage, zooplankton might migrate up and down between specific depths for similar reasons based on visibility. It might be beneficial to investigate the relationship between spectrum and migration to gain a better understanding of this phenomenon.

6. Symbols Used in Text

a Absorption coefficient m^{-1},

a_c^* chlorophyll-specific absorption coefficient,

a_g absorption coefficient of yellow matter m^{-1},

a_{other} absorption coefficient of other components (apart from pure water and chlorophyll) m^{-1},

a_w absorption coefficient of pure water m^{-1},

b scattering coefficient m^{-1},

C chlorophyll concentration $mg\ m^{-3}$,

c attenuation coefficient m^{-1},

$E_d(0^+)$ above-surface planar downwelling irradiance $W\ m^{-2}\ nm^{-1}$,

E_d planar downwelling irradiance $W\ m^{-2}\ nm^{-1}$,

E_u planar upwelling irradiance $W\ m^{-2}\ nm^{-1}$,

E_o scalar irradiance $W\ m^{-2}\ nm^{-1}$,

E_{od} scalar downwelling irradiance $W\ m^{-2}\ nm^{-1}$,

E_{od}^* a surrogate for E_{od} [see Eq. (6) and accompanying discussion] $W\ m^{-2}\ nm^{-1}$,

E_{ou} scalar upwelling irradiance $W\ m^{-2}\ nm^{-1}$,

K_d diffuse attenuation coefficient for the downwelling planar irradiance m^{-1},

L radiance $W\ m^{-2}\ nm^{-1}\ sr^{-1}$,

n_a index of refraction for air,

n_w index of refraction for water,

r distance m,

z geometric depth m,

β volume-scattering phase function,

$\tilde{\beta}$ normalized volume-scattering phase function,

λ wavelength nm,

μ cosine parameter, $\mu \equiv \cos\theta = \xi_3$,

$\bar{\mu}_d$ spectral downwelling average cosine,

θ_{Sun} Sun zenith angle deg,

ω_0 single-scattering albedo,

Ξ unit sphere: a set of all directions $\hat{\xi}$,

$\hat{\xi}$ unit vector,

ς optical depth.

References

1. A. Morel, "Optical modelling of the upper ocean in relation to its biogenous matter content (case 1 water)," J. Geophys. Res. **93,** 10,749–10,768 (1988).
2. C. D. Mobley, B. Gentili, H. R. Gordon, Z. Jin, G. W. Kattawar, A. Morel, P. Reinersman, K. Stamnes, and R. H. Stavn, "Comparison of numerical models for computing underwater light fields," Appl. Opt. **32,** 7484–7504 (1993).
3. C. D. Mobley, "A numerical model for the computation of radiance distributions in natural waters with wind-roughened surfaces," Limnol. Oceanogr. **34,** 1473–1483 (1989).
4. C. D. Mobley, *Light and Water: Radiative Transfer in Natural Waters* (Academic, San Diego, Calif., 1994).
5. C. D. Mobley, *Hydrolight 3.0 Users' Guide* (SRI International, Menlo Park, Calif., 1995).
6. C. D. Mobley, *Hydrolight 3.1 Users' Guide* (SRI International, Menlo Park, Calif., 1996).
7. R. K. Lowry, P. Machin, and R. N. Cramer, *BOFS North Atlantic Data Set: Oceanographic Data Collected during the North Atlantic Cruises of the National Environment Research Council Biogeochemical Ocean Flux Study (1989–1991)*; a UK Contribution to the Joint Global Ocean Flux Study (CD-ROM and Users's Guide) (British Oceanographic Data Centre, Proudman Oceanographic Laboratory, Birkenhead, England, 1994).
8. J. T. O. Kirk, *Light and Photosynthesis in Aquatic Ecosystems* (Cambridge U. Press, Cambridge, UK, 1994).
9. T. R. Anderson, "A spectrally averaged model of light penetration and photosynthesis," Limnol. Oceanogr. **38,** 1403–1419 (1993).
10. M. J. R. Fasham, J. L. Sarmiento, R. D. Slater, H. W. Ducklow, and R. Williams, "Ecosystem behaviour at Bermuda Station 'S' and Ocean Weather Station "India": a General Circulation Model and observational analysis," Global Biogeochem. Cycles **7,** 379–415 (1993).
11. J. Woods and W. Barkmann, "Simulating plankton ecosystems by the Lagrangian ensemble method," Philos. Trans. R. Soc. London Ser. B **343,** 27–31 (1994).
12. T. Platt and S. Sathyendranath, "Biological production models as elements of coupled, atmosphere–ocean models for climate research," J. Geophys. Res. **96,** 2585–2592 (1991).
13. R. W. Preisendorfer, "Generalized invariant imbedding relation," Proc. Natl. Acad. Sci. USA **47,** 591–594 (1961).
14. H. R. Gordon and A. Y. Morel, *Remote Assessment of Ocean Color for Interpretation of Satellite Visible Imagery: a Review* (Springer-Verlag, New York, 1983).
15. A. Morel, "Light and marine photosynthesis: a spectral model with geochemical and climatological implications," Prog. Oceanogr. **26,** 263–306 (1991).
16. L. Prieur and S. Sathyendranath, "An optical classification of coastal and oceanic waters based on the specific spectral absorption curves of phytoplankton pigments, dissolved organic matter, and other particulate materials," Limnol. Oceanogr. **26,** 671–689 (1981).
17. T. Tyrrell, P. M. Holligan, and C. D. Mobley, "Optical impacts of oceanic coccolithophore blooms," J. Geophys. Res. **104,** 3223–3241 (1999).
18. C.-C. Liu and J. Woods. "Prediction of ocean colour: Monte-Carlo simulation applied to a virtual ecosystem based on the Lagrangian ensemble method," in *Developing Space '98: Proceedings of the 1998 Remote Sensing Society Student Conference* (Remote Sensing Society, Nottingham, England, 1998), pp. 14–25.